Direct Measurements of *kT*-scale Capsule-Substrate Interactions & Deposition vs. Surfactant & Polymer Additives

Anna C. H. Coughlan,[1] *Isaac Torres-Diaz*,[1] *Huda A. Jerri*,[2,*] *and Michael A. Bevan*[1,*]
[1]Chemical & Biomolecular Engineering, Johns Hopkins University, Baltimore, MD 21218
[2]R&D Division, Firmenich Inc., Plainsboro, NJ 08536

*To whom correspondence should be addressed: huda.jerri@firmenich.com, mabevan@jhu.edu

I. Capsule-Substrate Interactions

Anisotropic colloidal capsules interact with a negatively charged glass slide by a three-dimensional surface force with the wall, u^{pw}, and one-dimensional body forces from external fields, u^{pf}, leading to a net interaction potential given as,

$$u(h,\psi)=u^{pw}(h,\psi)+u^{pf}(h) \tag{S1}$$

where h is the distance between the capsule and the surface and ψ is the capsule-coordinate polar angle (assuming no azimuthal angle dependence). Interaction potentials include superposition of contributions from electrostatics, u_E, van der Waals, u_V, depletion, u_D, steric, u_S, bridging, u_B , and gravity, u_G, as

$$u(h,\psi)=\left[u_E(h,\psi)+u_V(h,\psi)+u_D(h,\psi)+u_S(h,\psi)+u_B(h,\psi)\right]+u_G(h) \tag{S2}$$

Although the capsules in this study are somewhat anisotropic (*i.e.*, buckled spheres[1]), the well-depths, shapes and ranges of the above interaction potentials can be analyzed qualitatively and compared to the theory for spheres. For spherical capsules, there is no polar angle dependence in the potentials in Eq. (S2). To model the sphere-plate van der Waals potential, the rigorous Lifshitz theory for flat plates in conjunction with the Derjaguin approximation[2] can be fit with a convenient power-law expression for capsule-wall interactions as[3]

$$u_V(h)=-aA\left[h+\delta_V\right]^{-p} \tag{S3}$$

where a is capsule radius, A and p are fitting parameters, and δ_V is a correction for surface roughness.[4] Capsule-wall electrostatic interactions are given as,[5]

$$u_E(h)=B\exp(-\kappa h) \tag{S4}$$

$$B=64\pi\varepsilon a\left(\frac{k_BT}{e}\right)^2\tanh\left(\frac{e\Psi_p}{4kT}\right)\tanh\left(\frac{e\Psi_w}{4kT}\right) \tag{S5}$$

$$\kappa=\left(\frac{2CN_Ae^2}{\varepsilon k_BT}\right)^{0.5} \tag{S6}$$

where ε is the permittivity of water, k_B is Boltzmann's constant, T is absolute temperature, e is the elemental charge, ψ_p and ψ_w are the surface potentials of the capsule and the wall, κ^{-1} is the Debye length, C is the bulk electrolyte concentration, and N_A is Avogadro's number. For surfactant solutions, the Debye length is modified to account for micelle formation above the critical micelle concentration, C_{CMC}, as

$$\kappa=\left(e^2N_A/\varepsilon kT\right)^{1/2}\begin{cases}\left[\sum z_i^2C_i\right]^{1/2}, & C<C_{CMC}\\ \left[\sum z_i^2C_{CMC}+\left(C-C_{CMC}\right)\omega\right]^{1/2}, & C\geq C_{CMC}\end{cases} \tag{S7}$$

where z_i and C_i are the valence and concentration of surfactant anions and counter ions, and ω is the fraction of dissociated counter ions (estimated to be 0.25).[6]

The depletion attraction between a sphere and a flat surface can be described by an osmotic pressure term, $\Delta\Pi$, and an excluded volume, V_{EV}, the latter of which depends on the capsule and

surface geometry.[7-9] For dilute depletant concentrations, the interaction is non-zero when the distance between the colloid and the surface is less than the size of the depletant as

$$u_D(h) = \begin{cases} -\Delta\Pi V_{EV}(h) & h \le L \\ 0 & h > L \end{cases} \tag{S8}$$

where L is the diameter of the depletant, and $\Delta\Pi$ is obtained from compressibility factors for the depletant outside, Z_0, and inside, Z_0,the excluded volume region,[7]

$$\Delta\Pi = \rho_o k_B T\left[Z_o - Z_i K\right] \tag{S9}$$

where ρ_0 is the depletant number density outside the region, $K=\rho_0/\rho_i$, and ρ_i is the number density inside the excluded volume. At higher depletant concentrations, Eq. (S9) may not apply as the depletants no longer behave as an ideal solution and their concentration profile around capsules becomes oscillatory.[10] As a result, above certain volume fractions of the depletant, the potential of mean force between colloids is also oscillatory. In this case, the depletion interaction depends on the depletant concentration profile, which can be described as,[11]

$$u_D(h) = -k_B T\left[\Gamma(h) - \Gamma(\infty)\right] \tag{S10}$$

where $\Gamma(h)$ is the adsorbed amount of depletant per area and is a function of the position-dependent depletant number density. In surfactant solutions, the point at which depletion stabilization becomes significant can be qualitatively estimated by calculating the volume fraction of micelles from the following equation,

$$N_{agg} = \left([C] - CMC\right)/[M] \tag{S11}$$

where N_{agg} is aggregation number, equal to ~42 for SLES,[12] and C and M are the surfactant and micelle molar concentrations, respectively. Concentration M can be converted to volume fraction by assuming the SLES micelles have an approximate radius of 3nm.[13]

When macromolecules adsorb to a spherical capsule and a flat surface in a brush layer conformation, the system is considered symmetric and the repulsive steric interaction is[4]

$$u_S(h) = 16\pi a f_0 \delta_0 \left(\frac{\Gamma}{\gamma}\right) \exp\left(\frac{-h\gamma}{2\delta_0}\right) \tag{S12}$$

where f_0 and δ_0 are the free energy and thickness of the uncompressed brush, and Γ and γ are dimensionless constants used to fit unique brush architectures with varying density profiles normal to the surface.

The macromolecules could also bridge a tether between the capsule and substrate surfaces, causing an attractive interaction that is modeled as a Hookean spring,

$$u_B(h) = \frac{3Nk_B T}{4PL_T} h^2 \tag{S13}$$

where N is the number of tethers, assumed to be the same contour length L_T, and P is the persistence length of the macromolecule.

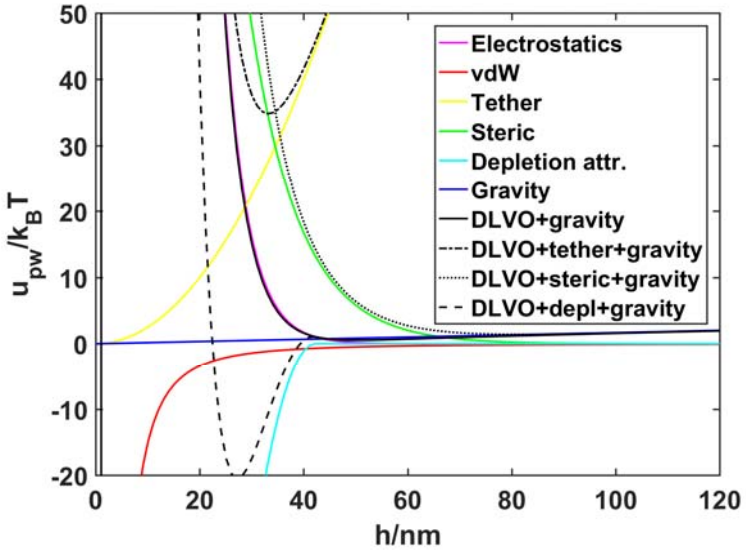

Figure S1: Example capsule-substrate potentials in a 30mM solution of SLES. The plots show the qualitative features of various spherical capsule-surface interactions that can be measured in TIRM. Since the exact theory for anisotropic buckled capsules is unknown for most of these potentials, the shapes and ranges of the spherical potentials shown in this figure can be used to analyze anisotropic-capsule substrate interaction potentials to deduce mechanisms that contribute to deposition or stabilization. The capsule parameters used to calculate the potentials are estimates of the real parameters of spherical capsules used in experimental test cases (see Base Case A in main text): a=15μm, $\psi_{p/w}$=-30mV and ρ_p=0.966 g/cm^3.

Given the orientation dependence of Eq. (S1), the form of the anisotropic-capsule surface interactions will not be the same as spheres. A recent theory solves the DLVO (electrostatic and van der Waals) interactions between an anisotropic capsule and a surface as a function of the Gaussian curvature at closest separation.[14] Steric interactions would also be valid given the assumptions of this anisotropic theory if the brush layer thickness is uniform laterally over the capsule surface. However, the tethering interaction would be dependent on colloidal geometry if the number of bridges in Eq. (S13) depends on the orientation of the capsule with respect to the surface. Similarly, the development of a theoretical form for orientation-dependent depletion interactions[15] between a capsule and a surface is an ongoing area of research.

The gravitational potential for a spherical capsule, which can also be approximated for buckled capsules using an effective a, is

$$u_g(h) = (4/3)\pi a^3(\rho_p - \rho_f)gh \tag{S14}$$

where ρ_p is capsule density, ρ_f is fluid density, and g is the gravitational constant. A summary plot depicting example theoretical spherical capsule-surface interactions is shown in Fig. S1. This plot serves as a guide for deducing mechanisms of anisotropic capsule deposition reported in this paper.

II. Microscopy Apparatus

To conduct Total Internal Reflection Microscopy (TIRM) measurements on capsules less dense than water, a laser was aligned with an adjustable mirror so that the laser beam hits the top of a glass prism at a 90º angle (see Fig. S2). In this set-up, the system is inverted compared to typical TIRM measurements,[2, 4] and the prism is placed on top of the slide, rather than the slide on top of the prism.

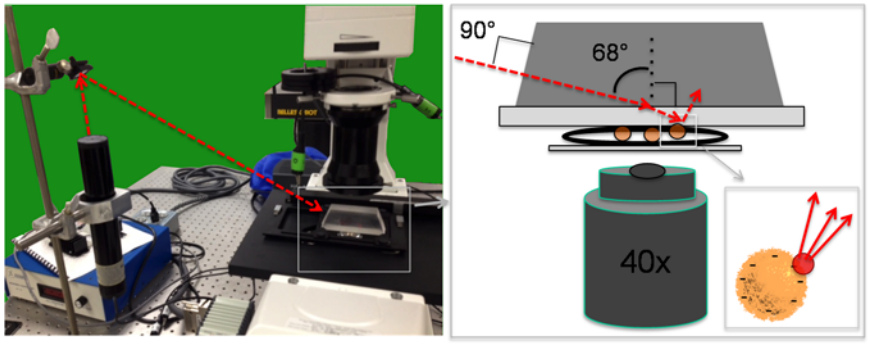

Fig. S2. Image and schematic of inverted Total Internal Reflection Microscopy (TIRM). A laser is mounted to the air table, and a mirror is oriented such that the laser is directed to hit the side of the prism at a 90º angle. The prism is placed on top of the glass slide. On the slide, an aqueous solution is contained in a black O-ring and coverslip. An evanescent wave is created at the glass-water interface, the intensity of which scales exponentially with distance from the interface. As such, the capsules interacting with the top surface of the slide scatter light that can be directly related to the distance of the capsule from the glass surface. Videos are taken that record the intensity of this scattering, to build a histogram of relative heights. The probability of relative heights can be used to calculate the interaction potential between the capsule and the glass slide via the Boltzmann equation, Eq. (5) in the main text.

III. SLES Solution Properties

To aid in the interpretation of the experimental results of capsule-surface interactions in SLES, the properties of the solutions were characterized as a function of SLES concentration. Shown in Fig. S3 is the Debye length and the micelle volume fraction as a function of SLES wt%, The electrostatic stabilization is more prominent at low concentrations of the surfactant: a greater Debye length indicates the repulsion is longer range. The figure also shows that micelle concentration increases to values above ~10% when the surfactant concentration is ~>1wt%.

IV. AAC Viscosity

The viscosity of three different solutions, 0wt% (DI water), 0.5 wt% and 1wt% AAC were measured (Cannon-Fenske routine viscometer, size 400, Cannon Instrument Company), and the data was fit to a trend line, from which the remaining viscosities at other concentrations were estimated. The results are shown in Fig. S4.

V. Spherical Capsules vs. Salt Concentration

Test cases were conducted of the inverted TIRM set-up (see Fig. S2), built for capsules that are less dense than water, to confirm proper alignment of the laser. These test cases were also conducted to ensure that core-shell capsule scattering of the evanescent wave follows the same theory used for silica and polystyrene,[2, 16-18] *i.e.* would be proportional to height, given that the capsules are a composite material. As such, TIRM was conducted in a simple salt solution for anionic polyurethane *spherical* capsules,[1] which are similar to the *buckled* LZ and HZ capsules used in the main text, to ensure that the potentials agreed with exact theory before exploring anisotropic surface interactions, for which exact theories have yet to be developed.

Fig. S5 shows example potential energy plots for two different individual spherical capsules. The capsule sizes were estimated by manually analyzing light microscopy images in ImageJ such that the only fitting parameters were capsule density, ρ, and zeta potential, ζ, which are displayed on the plots. Both fits to electrostatics and gravity (the capsules were not in the range

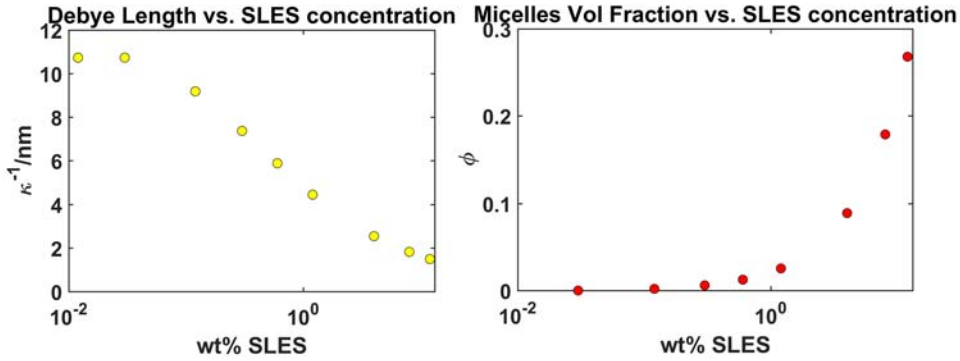

Fig. S3. Properties of SLES solutions. The Debye length calculated from Eq. (S6) and the volume fraction of micelles calculated from Eq. (S11).

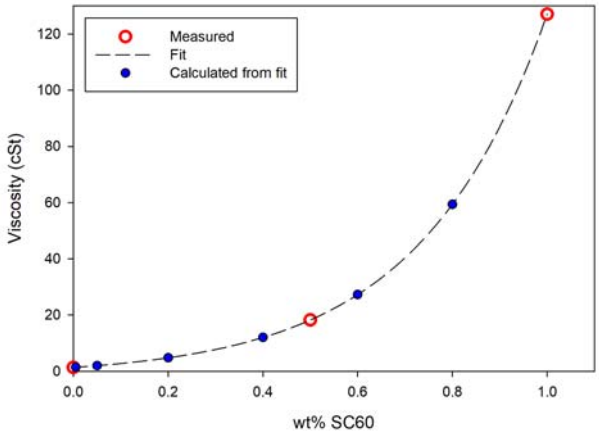

Fig. S4. Viscometer measurements and fit of viscosity as a function of wt% AAC polymer. The viscosity of DI water, 0.5wt% AAC, and 1wt% AAC were measured using a viscometer. The data were fit to a function of the form f = y0+a*exp(b*x), where y0=-1.732, a=3.10, b=3.726. The viscosities of other intermediate concentration solutions were then determined from this fit. To adjust for instrument measurement error, the viscosities shown in this plot were then rescaled/calibrated to the known viscosity of water, 0.9 cSt (the raw measurement for DI water was 1.37 cSt), for calculation of $\langle D_{\|} \rangle$ and then t_{FD}.

where van der Waals is significant) for these single particles produced similar theoretical parameters, indicating that the capsules have similar properties even if there is size polydispersity as a result of the capsule synthesis process. The plots also illustrate that the TIRM measurements are reliable since the fitting parameters are reasonable given previous knowledge and characterization of these capsules.[1] The potential energy results are also consistent over several capsules and trials.

VI. Buckled Capsules vs. Salt Concentration

Prior to analysis of buckled capsules in SLES and AAC solutions, capsule-surface interactions were first measured in the presence of salt, where only electrostatics and gravity apply (van der Waals are not significant, see Fig. S1 for an estimate of this range). Since the interaction potentials are relatively simple and the parameters in the theoretical equations for spheres are known and have already been fit to experimental data (Fig. S5), base case experiments in salt also provide a foundation for understanding how anisotropic effects impact the measured interactions as well as capsule scattering.

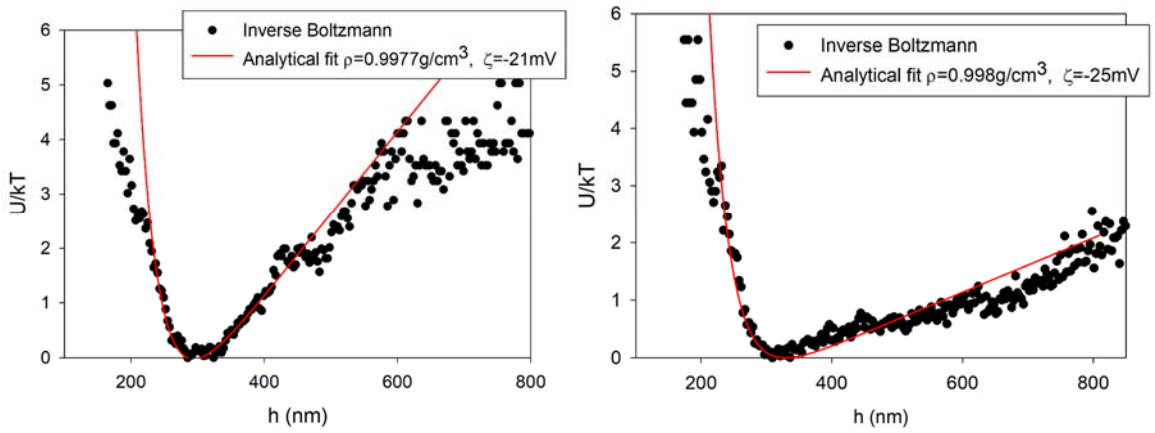

Figure S5: Potentials of spherical capsules interacting with a charged glass slide. Theoretical potentials that include electrostatic repulsion and the gravitational body force are fit to experimental measurements of two different spherical capsules in a 0.1mM NaCl solution interacting with a wall. The only fitting parameters are zeta potential, ζ, and capsule density, ρ, as the size was estimated by analyzing light microscopy images in ImageJ, where the capsule sizes are 2a=16.7 μm and 2a=12.3μm (from left to right).

Fig. S6 shows results for LZ capsules interacting with an above glass slide in aqueous media of DI water and 0.1 mM NaCl. Representative trajectories are plotted in the x-y plane (parallel to the slide) color-coded in time, and in z (normal to the slide) throughout the duration of the experiments, approximately 20 minutes. The trajectories correspond to the potential energy profiles, plotted on the scale of thermal energy, kT and normalized so that the most probable height, h_0, is at $u(h0)=0$. The profiles are calculated using the electrostatic and gravitational interactions and are equilibrium measurements, meaning they represent the average interaction between each capsule and the portion of the glass surface sampled by the capsule due to lateral diffusion. An image of the capsules in a LZ DI water experiment with the backlight on is shown in Fig. S6c, along with the corresponding evanescent wave scattering image for the same capsules in Fig. S6d.

The capsules in Fig. S6 are stable as is shown by the lateral diffusion in x and y. The capsules in DI water fluctuate in z much more than the capsule at 0.1 mM (bright green), as is most evident in Fig. S6b. This capsule at 0.1 mM is larger (confirmed via image analysis) and experiences a strong gravitational force towards the surface, and also has a steeper electrostatic repulsion since higher salt concentration shortens the Debye length (Eq. (S6)), which is further illustrated in the narrower potential plot in Fig. S6 for that capsule. The experimental potentials, shown in Fig. S6e and Fig. S6e, represent the superposition of energies, with the repulsion generally corresponding to the left-hand side and the attraction on the right-hand side. The solid lines are theoretical fits using electrostatics and gravity where the surface potentials for the capsules and the slide are assumed to be -60mV and the gravity is fit by finding the approximate size of the capsule with a capsule density of ρ_p =0.996 g/ml.

Theory does not fit to the DI water experiments, most likely due to shape-effects as the capsules are farther from the slide compared to the 0.1mM NaCl experiments (due to longer-range electrostatics), and can diffuse rotationally, sampling different orientations. As a result, the relation between intensity and position is more complex since orientation as well as height will affect intensity. On the other hand, the capsules closer to the slide in 0.1 mM solutions have limited rotational mobility, and therefore most likely remain in one orientation. Thus, the theoretical fit is more valid than it is in DI water, as can be seen by agreement between the solid green line and the

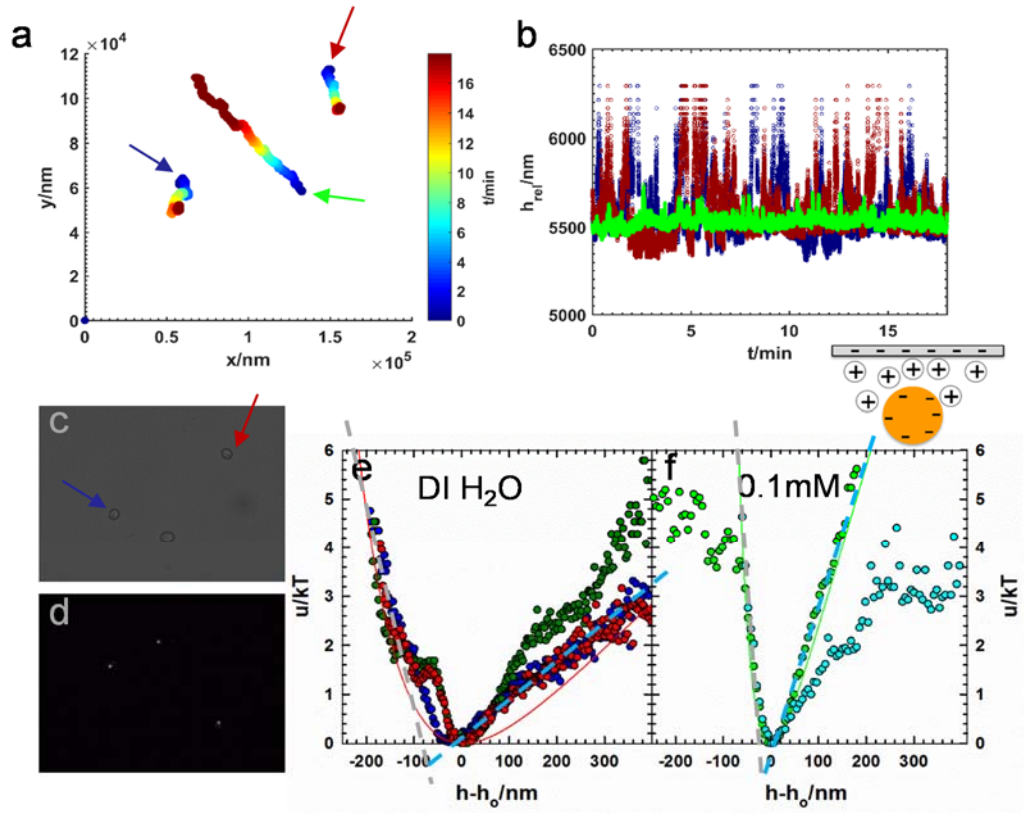

Fig. S6. LZ capsules are stable in low salt solutions due to electrostatic repulsion. (a) Trajectories of LZ capsules in DI water (red, blue) and in a 0.1 mM NaCl aqueous solution (green). (b) Trajectories in z for the same capsules, plotted as relative height, or distance, below the above glass surface, over a period of approximately 20 minutes. (c) A still image of the DI water experiment, showing two of the representative capsules, and the (d) corresponding scattering image of the same capsules when the backlight is turned off. The intensity of the capsules is only due to scattering of the evanescent wave. The results in (e) and (f) are the potentials for various individual capsules. It is shown that the capsules in the low salt solution have very broad electrostatics, although a theoretical potential for spheres that is the sum of electrostatics and gravity does not capture the whole experimental curves (as it did for spherical capsules, Fig. S5), most likely due to shape-effects. (f) A potential profile is fit to one of the experiments at 0.1 mM, at a diameter of 2a=19um, showing that at these conditions, the experiments follow the theory for spheres. The grey and blue dotted lines in (e-f) are shown as guides, and approximately represent how to interpret the repulsive and attractive sections of the potential energy plots. The slope of the grey line should increase with increasing salt, as observed, and the attraction should increase for larger capsules, as observed.

green points in Fig. S6f. It should be noted that at 1 mM NaCl, the LZ capsules all deposit on the glass slide (not shown).

Figure S7 shows trajectories and potentials for HZ capsules in DI water, 0.1 mM and 1 mM NaCl. HZ capsules are mostly stable at 1 mM, in contrast to LZ capsules, which all deposited. One of the capsules (color-coded as dark red) in 1 mM appears to be deposited laterally, but still diffuses in z. As a result of this trajectory, this capsule has the narrowest potential energy profile, shown in Fig. S7e. Similar to the DI water plots in Fig S6e, theoretical curves that include electrostatics and gravity (derived for spheres) do not fit to the experimental potentials shown in Fig. S6c because of the anisotropic nature of the capsules. Interestingly, potentials at 0.1 mM and 1 mM also show broad distributions, indicating that the theory for electrostatic repulsion for spheres does not apply

for HZ capsules, since the repulsion would be steeper at higher salt concentrations, a part of the theory for spheres that could be applied for the LZ capsules in Fig. S6. Only one of the experiments at 0.1 mM (bright red in Fig. S7d) seems to be close to the spherical theoretical potential for both gravity and electrostatics. The solid line in Fig. S7e shows that the capsule can be fit for gravity, but not electrostatics. An additional interaction such as steric repulsion could be affecting the HZ capsule results, particularly the non-agreement with the electrostatic theory for spheres.

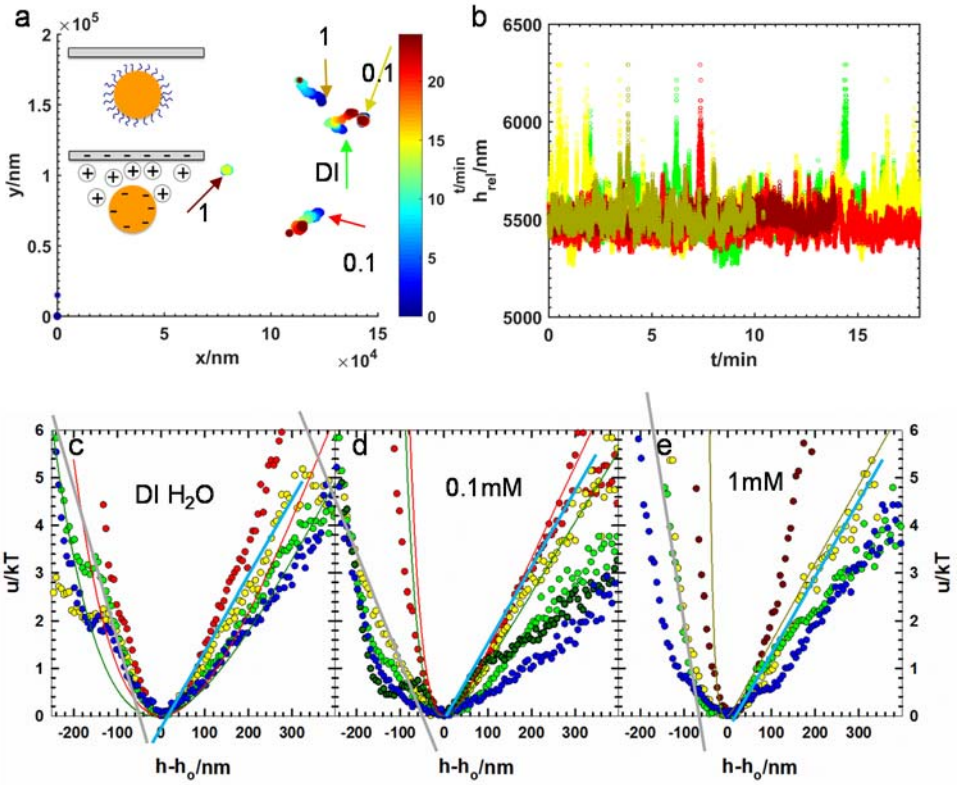

Fig. S7. HZ capsules are stable in low salt solutions due to electrostatic repulsion and possibly also due to steric repulsion from the polymer layer on the surface of the capsule. (a) Representative trajectories in the x-y plane for a capsule in DI water (green), capsules in a 0.1 mM NaCl solution (red and yellow) and capsules in a 1 mM NaCl solution (dark red and dark yellow). Some capsules appear to be stable at all three concentrations, while one capsule each at 0.1 mM (yellow) and 1 mM (dark red) are not diffusing laterally. Nevertheless, all of the capsules are diffusing in z (b), although the dark red capsule does appear to be deposited, and apparent fluctuations in z may be due to rotational diffusion instead. (c) Potential profiles of several unique capsules from TIRM experiments in DI water, showing broad distributions, which is to be expected at low salt, although the solid theoretical lines (electrostatics + gravity)) cannot capture the behavior, due to shape-effects. (d) The capsules also show broad potentials at 0.1 mM, and only one of the curves is close to the theoretical prediction from electrostatics (red line), which should get steeper with increasing salt, indicating the current theory for spheres is inadequate. (e) Potentials at 1 mM, at which the electrostatic repulsion should be very steep if it agreed with the theory for spheres. The theory for spheres matches gravity (solid dark yellow line), but does not predict the repulsion. The narrow dark red curve in (c) that corresponds to the dark red trajectories in (a-b) is indicative of a deposited capsule. The grey and blue lines in (c-e) are shown as visual guides, and approximately represent how to interpret the repulsive and attractive sections of the potential energy plots. The slope of the grey line should increase with increasing salt, which is *not* observed on average, while the attraction should increase for larger capsules, which *is* observed.

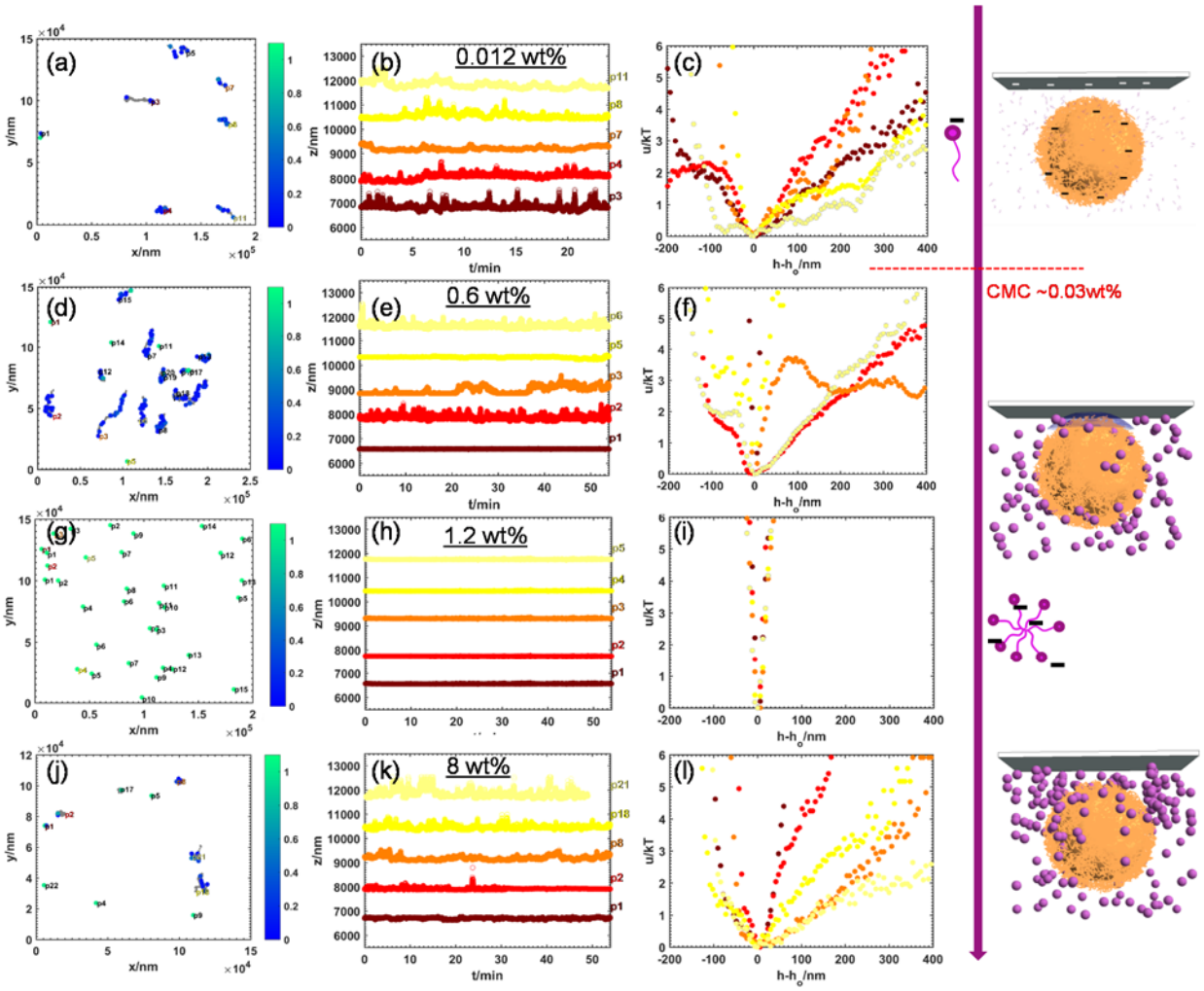

Figure S8: Trajectories and potential energies of several trials of LZ capsules at four different SLES concentrations representing the four main regimes. Capsule trajectories in the x-y plane are color-coded by the deposition lifetime parameter (Eq. (9) in the main text), and representative trajectories in height are shown along with the corresponding potential energy profiles for (a-c) 0.012wt% SLES, (d-f) 0.6wt% SLES (g-i) 1.2wt% SLES and (j-l) 8wt% SLES. At the lowest concentration below the CMC, the capsules are stable due to electrostatic repulsion. Above the CMC, the capsules begin to deposit due to the formation of micelles that causes a depletion attraction, and then at the even higher concentrations, the depletants start to pack around the capsule, causing oscillatory concentration profiles of the micelle and a barrier that causes kinetic depletion-induced stabilization.

VII. LZ Capsule Interactions & Deposition

The LZ capsules behave similarly to HZ capsules in both SLES and AAC solutions. Shown in Fig. S8-S9 are the analogous plots to the main Figs. 4 and 6, showing that the LZ capsules undergo depletion attraction and then relatively greater stabilization as a function of SLES and different tethering profiles at three different regimes of AAC.

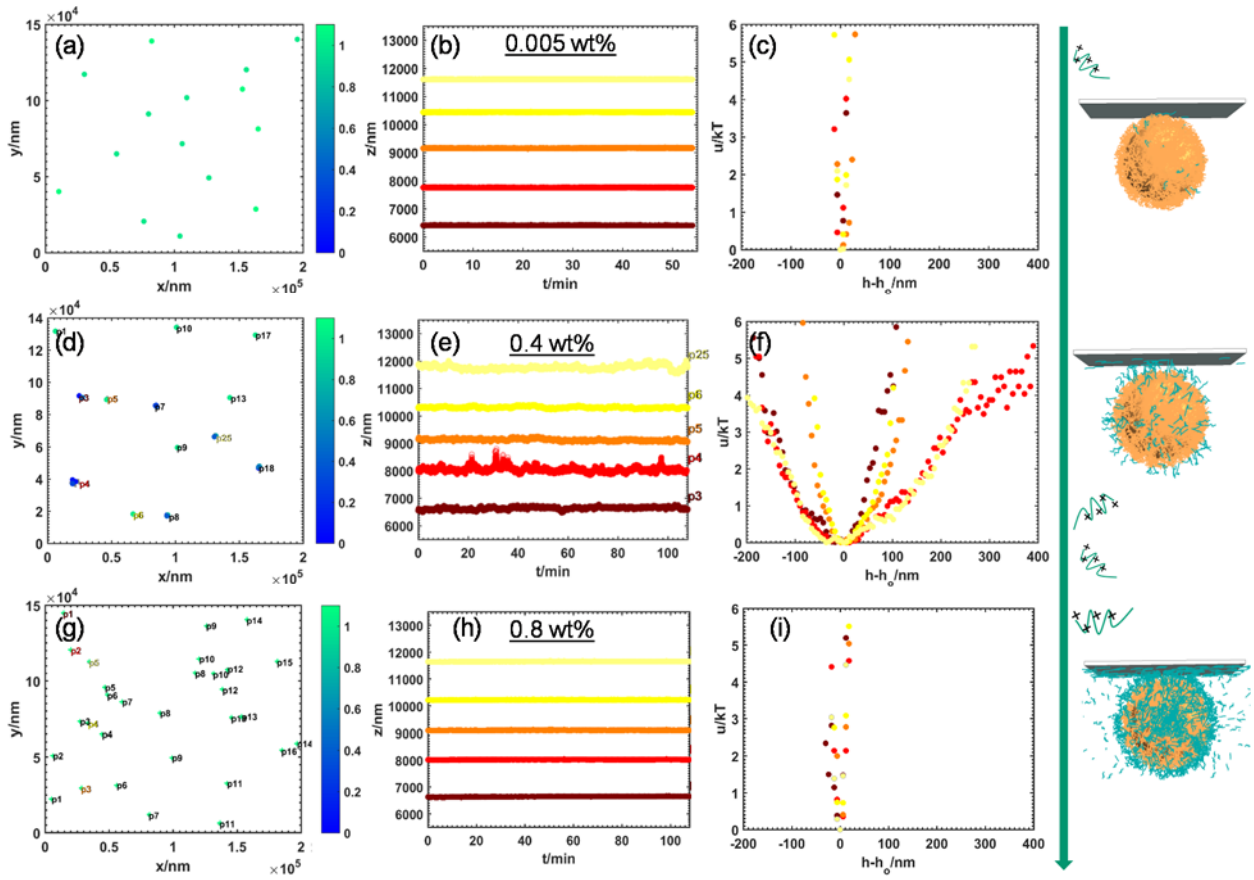

Figure S9: LZ capsules with AAC, representing the three main regimes. The planar trajectories, trajectories in z, and the corresponding potential energy profiles for (a-c) 0.005wt% AAC, (d-f) 0.4wt% SC 60 and (g-i) 0.8wt% AAC, showing that tethering occurs in all three regimes, but that the flexible, multiple chain tethers at 0.4wt% enable the capsules to diffuse in x, y and z. At the higher concentration, excess polymer in the bulk may also contribute to a depletion attraction in addition to the tight potential binding the capsules to the surface due to the tethers.

VIII. Deposition vs. Capsule Size

In order to investigate if there is a significant size dependence for deposition of the buckled capsules HZ and LZ, a size analysis was conducted for representative experiments. A band pass filter algorithm[19] was first applied in MATLAB to the light microscopy images to increase contrast levels, then the MATLAB function *bwboundaries* was applied to identify the capsule outlines. Capsule center is found by the average of all outline coordinates, then the radius is calculated from the average distance between the center and outline coordinates. The capsules identified and

tracked in the TIRM scattering videos are then matched to the capsules identified in the MATLAB-analyzed light microscopy images.

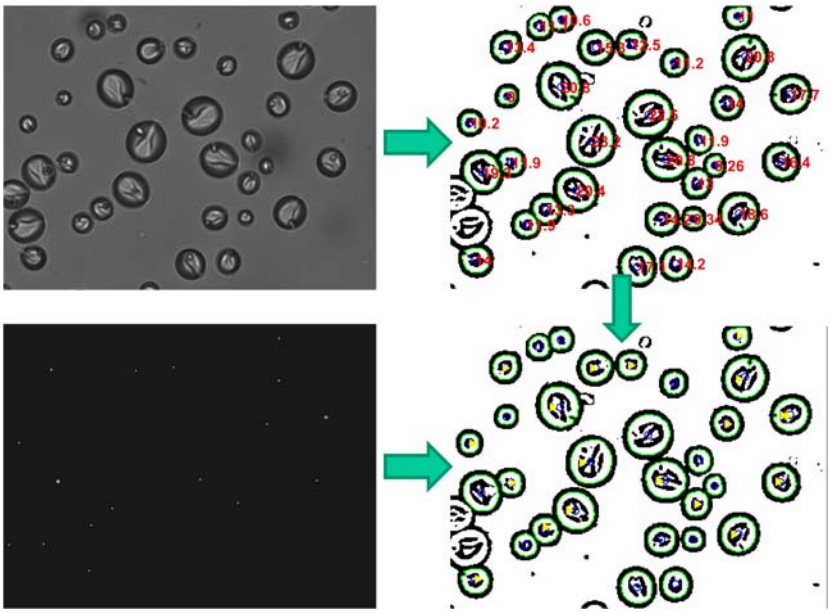

Figure S10. Sizing Polydisperse Capsules. To test whether capsule size impacts deposition, we have developed a capsule tracking code in MATLAB that sizes the capsules, then matches the capsules that were sized to those tracked in the TIRM scattering analysis. The code works as follows: (1) Application of a band pass filter to increase contrast. (2) Apply the MATBAL function *bwboundaries* to obtain the outlines (large green circles) of the capsules. The radii of the capsules that can be tracked are approximated by finding the center of the outlined shape (small blue circles), and then calculating the average distance from the center to all of the outline (green) pixels. Measured diameters are shown in red text, in μm. (3) The capsule tracking from the TIRM experiments picks up the scattering from the evanescent wave (see Fig. S1), which is a bright spot that is to the left of the real capsule center (bottom left image – note that this particular slice of the video does not track all of the capsules, but in the deposition algorithm, capsule coordinates are averaged over the whole video length and more are tracked than is shown in this slice). These coordinates from the TIRM analysis were then shifted, and matched to the previously tracked capsule centers (blue circles). All of the capsules that can be matched are marked with a yellow triangle.

All of the deposition lifetime plots in the main text ignore size effects in the calculation of deposition lifetimes, and it is assumed that the radius of the capsule does not influence the observed trends for both SLES and AAC, at least for the size distribution of these capsules (~10-20μm). However, it is evident by the theoretical capsule-surface potential energies, specifically electrostatics, depletion attraction, steric repulsion, and tethering that the capsule radius a either directly or indirectly affects the interaction strength. After sizing capsules from optical microscopy images (see Fig. S10), deposition lifetimes were calculated for representative experiments where each capsule's trajectory was analyzed using a unique $\langle D_{\|} \rangle$ (in Eq. (7)) as determined by the capsule size. Specific experiments were chosen for this analysis that represent intermediate regimes where both deposition and stability is observed to determine if deposition depends on capsule size. Figure S11 shows plots of deposition lifetimes as a function of capsule size for 3 SLES concentrations and 1 SC 60 concentration, showing no correlation or dependence with regards to capsule radius.

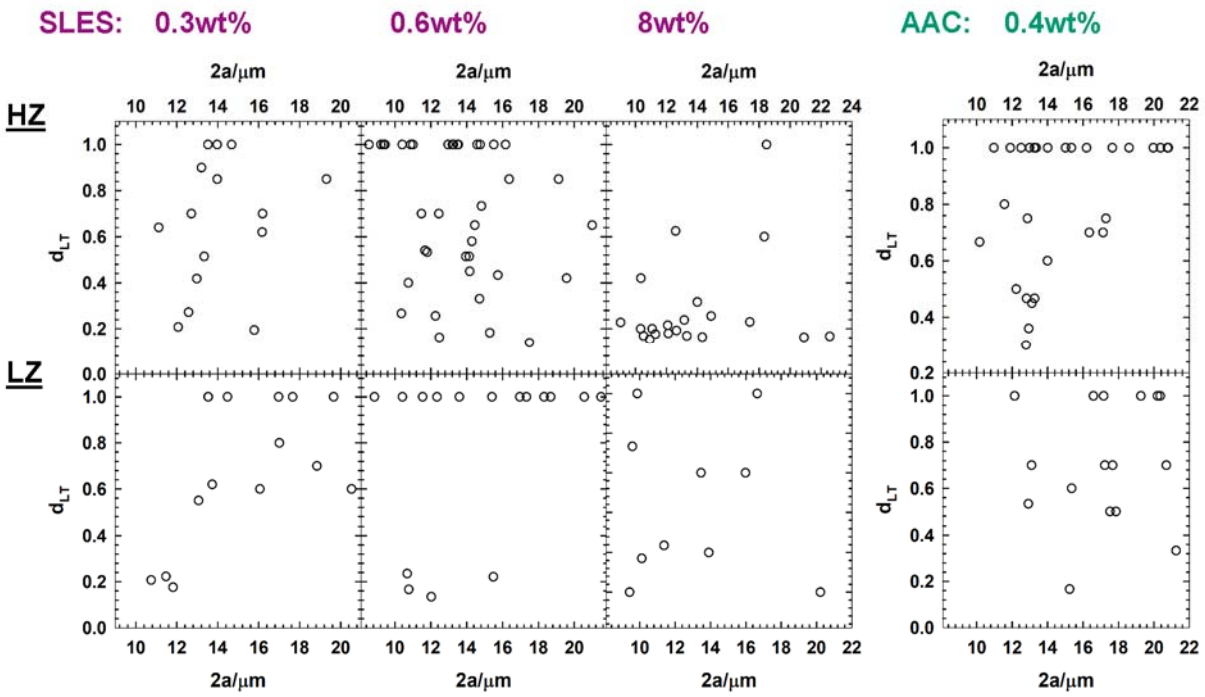

Fig. S11. Plots of the average deposition lifetimes measured for individual capsules, plotted against the sizes of the capsules, as determined by image analysis (for details, see Fig. S10). The concentrations shown are for intermediate cases where *both* deposition and stabilization occurred to see if size affected deposition. The results show that there is no obvious dependence on size, at least for this size range.

References

1. Jerri, H. A.; Jacquemond, M.; Hansen, C.; Ouali, L.; Erni, P. "Suction Caps": Designing Anisotropic Core/Shell Microcapsules with Controlled Membrane Mechanics and Substrate Affinity. *Advanced Functional Materials* **2016,** *26*, 6224-6237.
2. Bevan, M. A.; Prieve, D. C. Direct Measurement of Retarded Van Der Waals Attraction. *Langmuir* **1999,** *15*, 7925-7936.
3. Wu, H.-J.; Everett, W. N.; Anekal, S. G.; Bevan, M. A. Mapping Patterned Potential Energy Landscapes with Diffusing Colloidal Probes. *Langmuir* **2006,** *22*, 6826-6836.
4. Eichmann, S. L.; Meric, G.; Swavola, J. C.; Bevan, M. A. Diffusing Colloidal Probes of Protein–Carbohydrate Interactions. *Langmuir* **2013,** *29*, 2299-2310.
5. Russel, W. B.; Saville, D. A.; Schowalter, W. R. *Colloidal Dispersions*. Cambridge University Press: New York, **1989**.
6. Iracki, T. D.; Beltran-Villegas, D. J.; Eichmann, S. L.; Bevan, M. A. Charged Micelle Depletion Attraction and Interfacial Colloidal Phase Behavior. *Langmuir* **2010,** *26*, 18710–18717.
7. Edwards, T. D.; Bevan, M. A. Depletion-Mediated Potentials and Phase Behavior for Micelles, Macromolecules, Nanoparticles, and Hydrogel Particles. *Langmuir* **2012,** *28*, 13816-13823.
8. Yang, Y.; Edwards, T. D.; Bevan, M. A. Modeling Depletion Mediated Colloidal Assembly on Topographical Patterns. *Journal of Colloid and Interface Science* **2015,** *449*, 270-278.

9. Edwards, T. D.; Yang, Y.; Everett, W. N.; Bevan, M. A. Reconfigurable Multi-Scale Colloidal Assembly on Excluded Volume Patterns. *Sci. Rep.* **2015,** *5*, 13612.
10. Lekkerkerker, H. N. W.; Tuinier, R. *Colloids and the Depletion Interaction*. Springer: Berlin, **2011**; p 234.
11. Tuinier, R.; Vliegenthart, G. A.; Lekkerkerker, H. N. W. Depletion Interaction between Spheres Immersed in a Solution of Ideal Polymer Chains. *The Journal of Chemical Physics* **2000,** *113*, 10768-10775.
12. Aoudia, M.; Al-Haddabi, B.; Al-Harthi, Z.; Al-Rubkhi, A. Sodium Lauryl Ether Sulfate Micellization and Water Solubility Enhancement Towards Naphthalene and Pyrene: Effect of the Degree of Ethoxylation. *Journal of Surfactants and Detergents* **2010,** *13*, 103-111.
13. Banerjee, S.; Cazeneuve, C.; Baghdadli, N.; Ringeissen, S.; Leermakers, F. A. M.; Luengo, G. S. Surfactant-Polymer Interactions: Molecular Architecture Does Matter. *Soft Matter* **2015,** *11*, 2504-2511.
14. Torres-Díaz, I.; Bevan, M. A. General Potential for Anisotropic Colloid–Surface Interactions. *Langmuir* **2017,** *33*, 4356-4365.
15. Colón-Meléndez, L.; Beltran-Villegas, D. J.; Anders, G. v.; Liu, J.; Spellings, M.; Sacanna, S.; Pine, D. J.; Glotzer, S. C.; Larson, R. G.; Solomon, M. J. Binding Kinetics of Lock and Key Colloids. *The Journal of Chemical Physics* **2015,** *142*, 174909.
16. Prieve, D. C. Measurement of Colloidal Forces with Tirm. *Advances in Colloid and Interface Science* **1999,** *82*, 93-125.
17. Wu, H.-J.; Bevan, M. A. Direct Measurement of Single and Ensemble Average Particle−Surface Potential Energy Profiles. *Langmuir* **2005,** *21*, 1244-1254.
18. Augustin, M. A.; Hemar, Y. Nano- and Micro-Structured Assemblies for Encapsulation of Food Ingredients. *Chemical Society Reviews* **2009,** *38*, 902-912.
19. Crocker, J. C.; Grier, D. G. Methods of Digital Video Microscopy for Colloidal Studies. *Journal of Colloid and Interface Science* **1996,** *179*, 298-310.